Chemistry–A European Journal
Research Article
doi.org/10.1002/chem.202403097
Chemistry Europe
European Chemical Societies Publishing
www.chemeurj.org

Stable Antiaromatic [16]Triphyrin(2.1.1) with Core Modification: Synthesis Using a 16π Electrocyclic Reaction

Yuya Hirai,[a] Yosuke Kawazoe,[a] and Ken-ichi Yamashita*[a, b]

Antiaromatic porphyrinoids have attracted significant attention owing to their unique electronic properties and potential applications. However, synthesis of antiaromatic contracted porphyrinoids is challenging owing to the inherent instability associated with smaller ring sizes. In this study, we report the synthesis and characterization of the first stable trioxa[16]triphyrin(2.1.1), a novel 16π antiaromatic contracted porphyrinoid. We utilized a core modification approach to stabilize the [16]triphyrin(2.1.1). X-ray crystallographic analysis revealed a nearly planar structure. Electrochemical studies demonstrated reversible oxidation behavior and a small HOMO–LUMO gap, which was consistent with its antiaromatic nature. Chemical oxidation yielded an aromatic [14]triphyrin(2.1.1) dication, highlighting the antiaromaticity–aromaticity switching capability of this system. This synthesis involved the discovery of a key intermediate, dihydrotrioxatriphyrin(2.1.1), which underwent oxidative dehydrogenation to yield the target compound. Theoretical calculations suggested that dihydrotrioxatriphyrin(2.1.1) formed via a rare 16π electrocyclic reaction. The successful synthesis and characterization of this stable trioxa[16]triphyrin(2.1.1) underscores the potential of the core modification strategies for the rational design of novel antiaromatic systems with tunable properties. Moreover, the discovery of the rare 16π electrocyclic reaction advances the understanding of high-order pericyclic processes and may inspire new synthetic strategies for complex macrocyclic compounds.

Introduction

Antiaromaticity, a phenomenon where 4 nπ cyclic conjugated molecules exhibit destabilizing electronic structures, has attracted significant interest because of their unique chemical and physical properties.[1] Antiaromatic destabilization decreases with increasing ring sizes, rendering porphyrinoids, which are representative large π-conjugated macrocycles that are readily synthesized, amenable for pronounced antiaromaticity.[2–4] Antiaromatic porphyrinoids range from isophorins, 2-electron-reduced 20π porphyrins,[5,6] to expanded porphyrinoids such as hexaphyrins. However, reports of antiaromatic contracted porphyrinoids are scarce, with the exception of norcorroles.[7] This scarcity could be attributed to the inherent instability associated with smaller ring sizes.[8,9]

Consequently, the development and characterization of antiaromatic-contracted porphyrinoids remains a significant challenge. Among the contracted porphyrinoids, triphyrin(2.1.1)s are promising scaffolds because of their facile synthesis.[10–12] Typically, triphyrin(2.1.1)s exhibit 14π aromaticity (Figure 1a), and therefore, their 2e-reduced forms are expected to exhibit antiaromaticity owing to the resulting 16π cyclic conjugated system (Figure 1b). However, substantial steric repulsion between hydrogen atoms inside the macrocycle is expected. Hence, the synthesis of parent [16]triphyrin(2.1.1) has not yet been achieved, and only a few derivatives containing B(III) or other atoms at the center of the macrocycle have been synthesized to relieve steric hindrance. Notably, Latos-Grażyński et al. reported a thiophene-annulated B(III)-[16]triphyrin(2.1.1) derivative in 2014 (Figure 1c), representing the first antiaromatic triphyrin(2.1.1).[13] Subsequently, similar annulated B(III)-triphyrin(2.1.1)s have been reported, which are believed to be

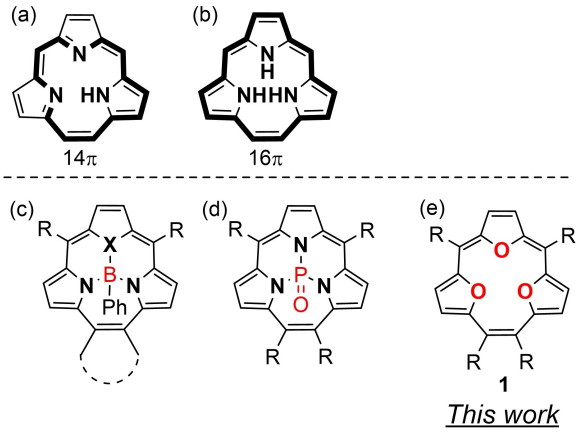

Figure 1. Parent structures of (a) 14π aromatic and (b) 16π antiaromatic triphyrin(2.1.1)s. Structures of antiaromatic [16]triphyrin(2.1.1) analogs reported previously (c and d) and studied in this work (e).

[a] Y. Hirai, Y. Kawazoe, K.-i. Yamashita
Department of Chemistry, Graduate School of Science, Osaka University,1-1 Machikaneyama, Toyonaka, Osaka 560-0043, Japan
E-mail: yamashita-k@chem.sci.osaka-u.ac.jp
[b] K.-i. Yamashita
Innovative Catalysis Science Division, Institute for Open and Transdisciplinary Research Initiatives (ICS-OTRI), Osaka University, Suita, Osaka 565-0871, Japan

Supporting information for this article is available on the WWW under https://doi.org/10.1002/chem.202403097

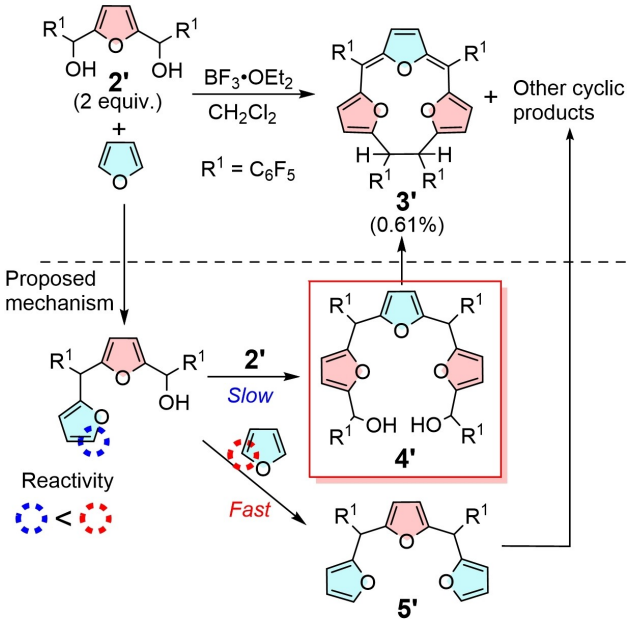

Scheme 1. Unexpected acid-catalyzed reaction affording a dihydrotrioxatriphyrin(2.1.1) **3′** as a byproduct, and its proposed reaction mechanism.

stabilized by π-extensions attributed to annulation.[14–16] Attempts to synthesize an antiaromatic triphyrin(2.1.1) analog without annulation resulted in a nonaromatic dihydrotriphyrin(2.1.1).[17] The first stable [16]triphyrin without annulation was synthesized via phosphorus complexation (Figure 1d).[18] To date, no other examples have been reported.

In this study, we aimed to synthesize stable 16π antiaromatic triphyrin(2.1.1)s using a strategy distinct from complexation. We utilized a core modification approach that involves heteroatom substitution, wherein the nitrogen atoms in the ring are replaced by oxygen atoms (Figure 2).[19,20] Prior studies have shown that core-modified isophlorins eliminate the steric repulsion among the inner hydrogen atoms, resulting in strong antiaromaticity and stabilization.[5,21] Expecting a similar benefit, we synthesized a core-modified [16]triphyrin(2.1.1), trioxa[16]triphyrin(2.1.1) (**1**, Figure 1e), and evaluated its antiaromaticity. Although there have been several reports on the single-atom core modification of triphyrin(2.1.1)s,[11,13–16,22] no reports exist on their double or multiple core modifications, rendering **1** the first of its kind.

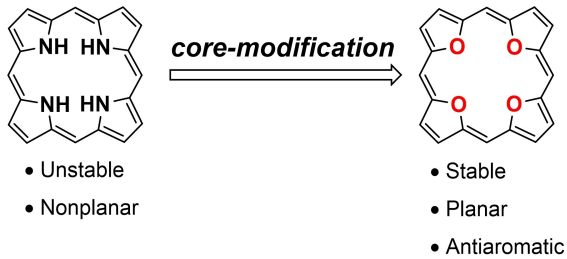

Figure 2. Core-modification approach to stabilize 20π antiaromatic isophlorins.

Results and Discussion

Preliminary Experiments and Synthetic Strategy

Triphyrins(2.1.1) have traditionally been synthesized via the acid-catalyzed [2 + 1] condensation[14,23,24] or McMurry coupling of tripyrroles.[10,11,17,22,25] In this study, we incorporated a novel cyclization reaction into our synthetic strategy that was serendipitously discovered during the synthesis of another compound. First, we describe this unexpected reaction, which guided the determination of the synthetic route for **1** (Scheme 1). During the synthesis of a tetraoxaisophorin[21] via the acid-catalyzed [2 + 2] condensation of furan and 2,5-bis(arylhydroxymethyl)furan **2′**, we unexpectedly observed the formation of dihydrotrioxatriphyrin **3′** as a minor byproduct, as evidenced by MALDI-MS spectrometry (Figure S4) and ^{1}H NMR (Figure S5).

During the formation of **3′**, the trifuran **4′** was presumed to be an intermediate arising from the [2 + 1] condensation of two molecules of **2′** and one molecule of furan. Based on this assumption, attempts were made to optimize the reagent stoichiometry; however, the resulting yield of **3′** was only 0.6 %. This low yield was attributed to the likely preferential formation of byproduct **5′**, which outcompeted the desired cyclization pathway. In the difuran intermediate, which is presumed to form in the initial stage of the reaction, the free α-position of the furan ring is deactivated by the electron-withdrawing effect of the R^1 substituent, making it less reactive compared to the α-position of an unsubstituted furan. As a result, the formation of **5′** is favored over the that of **4′**. Therefore, we hypothesized that the selective synthesis of **4** followed by cyclization would afford **3** in a higher yield. The final target compound **1** could then be obtained through the oxidative dehydrogenation of **3**.

Synthesis and Characterization

Trioxa[16]triphyrin(2.1.1) **1** was synthesized as shown in Scheme 2. To facilitate the preparation of the starting material **2**, 3,5-bis(trifluoromethyl)phenyl groups were selected as R^1 substituents. Condensation of **2** with 20 equiv. of furan catalyzed by BF_3·OEt_2 afforded the trifuran **5**, which underwent subsequent Friedel–Crafts acylation to yield **6**. The reduction of **6** with $NaBH_4$ afforded **4**, which served as the precursor for cyclization.

Cyclization reaction of **4** was performed by treatment with BF_3·OEt_2 in CH_2Cl_2 at room temperature. The ^{1}H NMR spectrum of the crude product (Figure S6) exhibits broad peaks attributed to structurally uncertain by-products, along with evident peaks corresponding to the target compound **3**. Purification of the crude product afforded the desired cyclic product **3** in 7 % yield.

The connectivity and composition of **3** was confirmed by NMR and ESI-HRMS analyses. ^{1}H NMR spectrum of **3** is shown in Figure 3. All ^{1}H NMR signals in **3** are assigned using 2D NOESY NMR measurements (Figure S7). The singlet signal for a proton on the *meso*-carbon with an R^2 substituent was observed at 5.14 ppm. However, no signal was observed for a proton on the

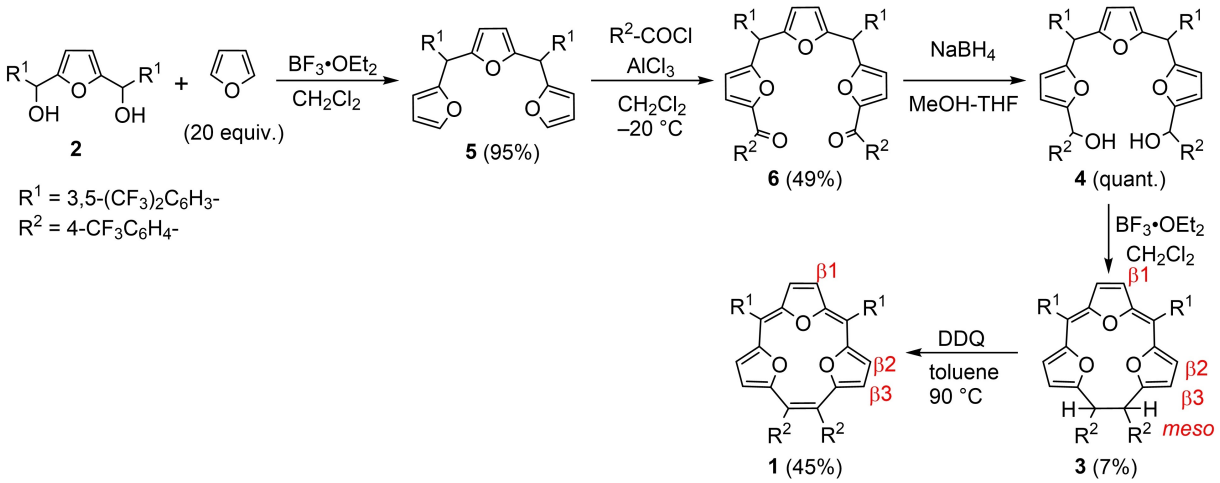

Scheme 2. Synthetic route to trioxa[16]triphyrin(2.1.1) **1** via dihydrotrioxatriphyrin(2.1.1) **3**.

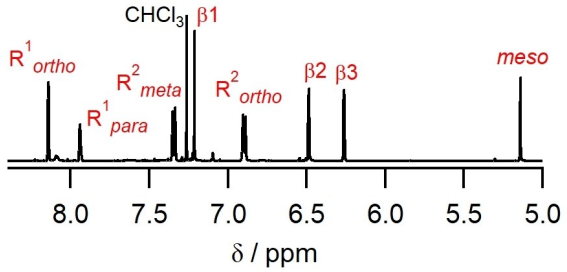

Figure 3. ^{1}H NMR (500 MHz, $CDCl_3$) spectrum of **3**.

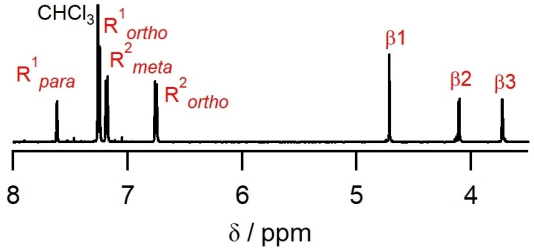

Figure 4. ^{1}H NMR (500 MHz, $CDCl_3$) spectrum of **1**.

meso-carbon with the R^1 substituent, supporting the proposed structure of **3**.

In the cyclic product **3**, the central furan skeleton adopts a quinoid structure, suggesting the extension of π-conjugation throughout the molecule. Notably, the absorption spectrum of **3** extends to the long wavelength region near 500 nm (Figure S8), corroborating the extended π-conjugation.

Compound **3** possesses two stereogenic centers (*meso*-carbons bearing an R^2 substituent), giving rise to the possibility of two diastereomers (*syn* and *anti*). However, the ^{1}H NMR spectrum of **3** indicated the presence of only a single diastereomer. Although the *syn* isomer lacked mirror symmetry owing to the axial-equatorial orientation of the two R^2 substituents, the *anti* isomer exhibited C_2 symmetry with an axial–axial or equatorial–equatorial orientation of the two R^2 substituents. The ^{1}H NMR spectrum suggested a symmetric structure, implying that the *anti* isomer was formed selectively.

Trioxa[16]triphyrin(2.1.1) **1** was obtained by the oxidation of **3** with 2,3-dichloro-5,6-dicyano-1,4-benzoquinone (DDQ) in toluene at 90 °C. The ^{1}H NMR spectrum of **1** is shown in Figure 4. All ^{1}H NMR signals in **1** are assigned using 1D NOESY NMR measurements (Figure S10). No *meso*-proton signals were observed. Signals for the β1, β2, and β3 protons were detected at 4.71, 4.10, and 3.73 ppm, respectively. These signals exhibited significant upfield shifts compared to **3**. This upfield shift is attributed to the shielding effect of the magnetic field generated by the paramagnetic ring current of the antiaromatic compound, indicating the antiaromatic nature of **1**. The observed chemical shifts of **1** are similar to those reported previously for [16]triphyrin.[18]

Trioxa[16]triphyrin(2.1.1)**1** showed good stability, with no significant spectral changes observed for at least a few days when stored in the dark. Of note, we initially investigated a derivative of **1** with $-C_6H_5$ groups as R^2 substituents. This derivative was prone to oxidation under ambient conditions. When left in solution, the derivative showed NMR peak broadening, likely because of single-electron oxidation, as well as the appearance of new peaks. Additionally, mass spectrometry revealed peaks suggestive of oxygen adduct formation. These decomposition processes could be partially suppressed by shielding the compound from light. These observations indicate that the CF_3 groups in **1** contribute to its stability against oxidation. This enhanced stability can be attributed to the electron-withdrawing nature of the CF_3 groups, which increase the oxidation potential of the triphyrin core.

X-Ray Structural Analyses

Single crystals of **1** were obtained by vapor diffusion of methanol into an acetone solution. X-ray diffraction measurements revealed that the crystal contained two crystallographically independent molecules (A and B). The molecular structures

of A and B are shown in Figure 5 and Figure S1, respectively. Molecules A and B exhibit nearly planar conformations (Figure S3) with small mean plane deviation values defined by the O_3C_{16} atoms (0.13 and 0.19 Å for A and B, respectively).

The bond lengths within the macrocycle for A and B are shown in Figure 6 and Figure S2, respectively, revealing a considerable bond length alteration pattern. The C15=C16 bond lengths of 1.373(3) and 1.367(4) Å in molecules A and B were shorter than the adjacent C_{meso}–C_α bonds (1.464–1.467 Å). This observation indicates the presence of a localized double bond between the two *meso*-positions and suggests that among the two possible valence tautomers of **1** derived from bond alternation, the structure shown in Figure 1(e) is predominant.

The inter-oxygen distances within **1** are short, especially O1···O2 and O2···O3, at approximately 2.46 Å. These are the shortest reported intramolecular distances in crystal structures of oxaporphyrinoids reported to date, and only one of them has been reported to be relatively short.[26] This geometry was also reproduced by quantum chemical calculations at the CAM–B3LYP/6-311G(d,p) level of theory. The charges of the oxygen atoms are expected to be negative as a result of their electronegativity, which was confirmed by natural bond orbital (NBO) charge analysis (Figure S12) and calculation of an electrostatic potential map (Figure S13). The negative charges on the oxygen atoms would destabilize the planar structure through electrostatic repulsion. However, the observed structure maintained a relatively high degree of planarity. Although the reason for this has not been fully elucidated at this time, we propose the possibility of chalcogen bonding[27–29] between oxygen atoms. Chalcogen bonding, a type of sigma-hole interaction, is generally not observed between oxygen atoms because of the high energy level of the σ* orbital. However, recent theoretical and experimental reports have suggested interactions involving σ-holes in the oxygen atoms.[30–33] In **1**, the inter-oxygen distances are shorter than the sum of the van der Waals radii and previously reported experimental distances for oxygen–oxygen interactions.[30–32] In addition, chalcogen bonding is known for its directionality, in which case, the C_α–O1A–O2A, C_α–O3A–O2A, and C_α–O1B–O2B angles are approximately 160°. These geometrical features potentially allow for interaction between the σ* orbitals of C_α–O1 or C_α–O3 and the lone pair of O2. Furthermore, NBO calculation of the geometry-optimized structure revealed the presence of these geometrically expected interactions with a stabilization energy $E(2) \approx 0.6$ kcal/mol (Figure S14). Further analysis of this intriguing structural feature is currently underway.

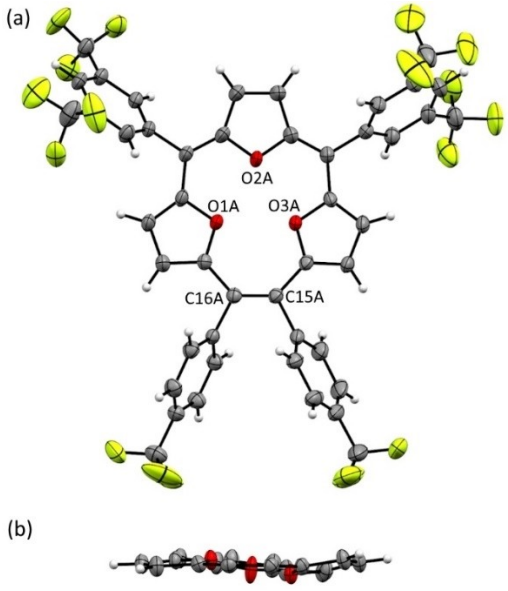

Figure 5. Crystal structure of **1** (Molecule A) (C = black, H = white, O = red, and F = yellow). Thermal ellipsoids are drawn at 50% probability level. (a) Top view, (b) side view without aryl substituents.

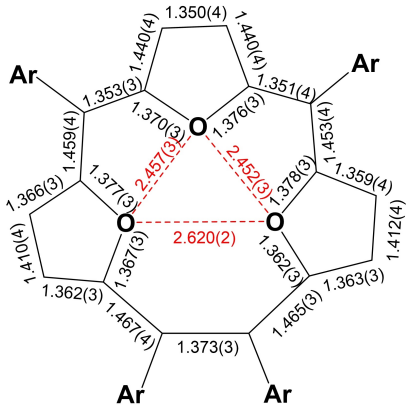

Figure 6. Selected bond lengths and distances (Å) of the crystal structure of **1** (molecule A).

Theoretical Calculations

To gain further insights into the antiaromaticity of **1**, we calculated the nucleus-independent chemical shift (NICS)[34,35] and anisotropy of the induced current density (AICD).[36] To simplify the calculations, we performed the calculation on a model compound **1**†, where all the trifluoromethyl groups of **1** were replaced by hydrogen atoms. The NICS(0) and $NICS_{zz}(0)$ values at the center of **1**† calculated at the GIAO-CAM–B3LYP/6-311 + G(2d,p)//CAM–B3LYP/6-311G(d,p) levels were 17 and 63 ppm, respectively. These large positive values strongly supported the antiaromatic character of **1**.

Furthermore, the AICD plot for **1**† reveals a counterclockwise ring current (Figure 7), which is a characteristic feature of antiaromatic π-systems. The contribution of the $C_{\beta\text{-}furan}$ atoms to the ring current was relatively small, whereas the oxygen atoms played a dominant role in sustaining the antiaromatic ring current.

Spectroscopic Properties

The UV/Vis/NIR absorption spectrum of **1** are shown in Figure 8a. The maximum absorption wavelength of **1** was 318.5 nm, which was remarkably shorter than that of **3**

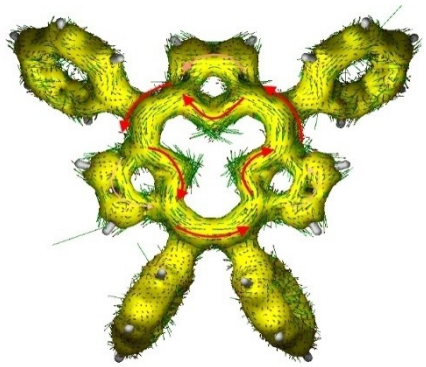

Figure 7. Anisotropy of the induced current density (AICD) plot for $\mathbf{1}^{\dagger}$ (isosurface value: 0.05).

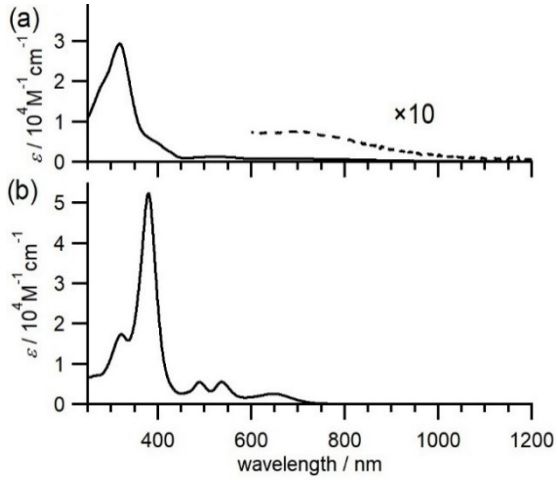

Figure 8. UV/vis/NIR absorption spectra of (a) **1** and (b) $\mathbf{7}^{2+}$ in acetonitrile.

(500 nm). Compound **1** also exhibited a relatively weak and broad absorption band at approximately 518 nm ($\varepsilon \approx 1000$) and a significantly weak broad peak extending to approximately 1100 nm.

The presence of weak, broad absorption bands in the visible and near-infrared regions could be attributed to the small HOMO–LUMO gap in antiaromatic systems. The forbidden nature of the HOMO–LUMO transition resulted in low oscillator strengths and molar absorption coefficients for these absorption bands.

Electrochemistry

The electrochemical properties of **1** were examined using cyclic and differential pulse voltammetry (CV, and DPV) (Figure S11). The cyclic voltammogram of **1** revealed two reversible oxidation waves at 0.12 and 0.46 V (vs. Fc/Fc^{+}), indicating the stability of the oxidized species and the ability of the compound to undergo multiple electron-transfer processes.

In contrast, the reduction wave was observed irreversibly at −1.59 V, suggesting that the reduced species was relatively unstable or underwent a rapid chemical transformation following the electron transfer.

Notably, the HOMO–LUMO gap of **1**, estimated from the difference between the first oxidation and reduction potentials determined by DPV, was −1.59 eV. This value was comparable to that of the previously reported [16]triphyrin(2.1.1) (−1.69 eV),[18] and was significantly smaller than those of aromatic [14]triphyrin(2.1.1) derivatives.[10,18] The small HOMO–LUMO gap was consistent with the extended absorption spectrum of **1**.

Oxidation of 1 Affording a [14]triphyrin(2.1.1) Dication

The low oxidation potentials of **1** prompted us to investigate the formation of a two-electron oxidized product $\mathbf{7}^{2+}$, which is expected to exhibit 14π aromaticity, by the oxidation of **1** (Scheme 3). When **1** was treated with $NOPF_6$ in acetonitrile, the ^{1}H NMR and absorption spectrum of the product indicated the formation of $\mathbf{7}^{2+}$, as anticipated. The ^{1}H NMR peaks for the β-protons are significantly downfield-shifted to 10.16, 10.11, and 9.56 ppm (Figure 9), indicating an antiaromaticity-to-aromaticity reversal upon oxidation.

The UV/Vis absorption spectrum of $\mathbf{7}^{2+}$ (Figure 8b) exhibits a sharp and intense absorption band at 380 nm ($\varepsilon \approx 52000$) and multiple weak absorption bands in the 450–600 nm region ($\varepsilon \approx 10^3$), resembling the spectral features of previously reported 14π aromatic triphyrin(2.1.1) derivatives.[10,11]

Reaction Mechanism of the Cyclization Reaction Affording 3

Finally, we investigated the reaction mechanism of the cyclization reaction from **4** to **3** using quantum chemical calculations. A plausible reaction mechanism is illustrated in Scheme 4. The Lewis acid catalyst promotes the elimination of

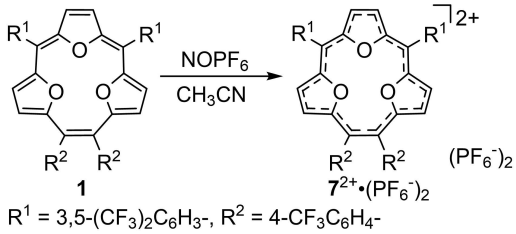

Scheme 3. Oxidation of **1** affording a [14]triphyrin(2.1.1) dication $\mathbf{7}^{2+}$

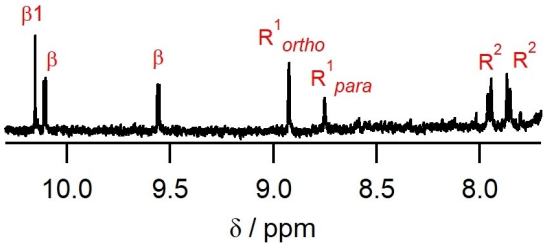

Figure 9. ^{1}H NMR (500 MHz, CD_3CN) spectrum of $\mathbf{7}^{2+}$.

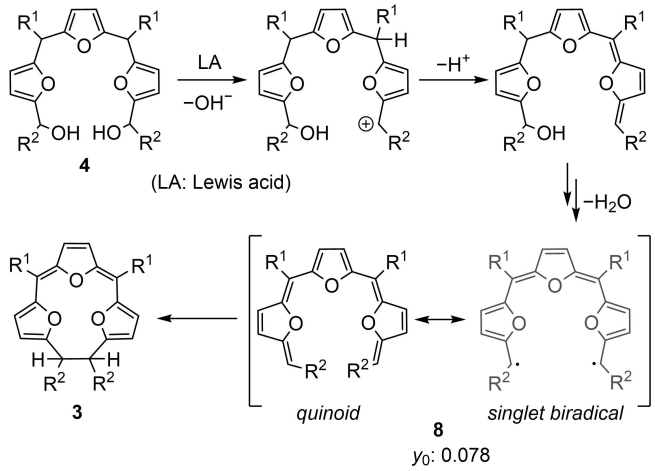

Scheme 4. Proposed reaction mechanism for cyclization reaction of **4** affording **3**.

the hydroxyl group, generating a carbocation, which is similar to typical porphyrin formation reactions. Subsequently, a proton was eliminated from the *meso*-carbon bearing the electron-withdrawing R^1 substituent, resulting in the formation of an intermediate with the loss of a water molecule from compound **4**.[37] The repetition of this reaction led to the elimination of another water molecule, yielding the 16π linear-conjugated intermediate **8**. The cyclization reaction proceeded from **8** to afford cyclized product **3**.

Ten geometric isomers of **8** are derived from the four $C_{meso}=C_{\alpha}$ double bonds (Table 1). Among these, only three isomers, *ZZ-ZZ*, *ZZ-ZE*, and *ZZ-EE* (See Table 1 for configuration notations), have conformations that can undergo the reaction based on close distance between the carbons involved in bond formation (*dist*). Initially, we performed a conformational search for geometric isomers of **8**†, replacing all trifluoromethyl groups in **8** with hydrogen atoms, using a combination of the CENSO[38] and CREST[39,40] program developed by Grimme. By comparing the energies of the most stable conformers of each geometric isomer (Table 1, Figure S15), we found the *ZZ-ZZ* isomer to be the most stable. In the structure of all obtained conformers of *ZZ-ZZ*-**8**†, the aryl groups at the end of the molecule (R^2) and the furan moieties are stacked in a π–π manner (Figure 10). This interaction is considered one of the stabilizing factors. In the most stable conformer of *ZZ-ZZ*-**8**†, the distance between the carbons involved in bond formation (*dist*) was 3.707 Å. The *ZZ-EZ*-**8**† and *ZZ-EE*-**8**† also exhibited close C···C distance in their most stable conformers.

We hypothesized that intermediate **8** might possess a quinoid structure in the closed-shell state. However, owing to the extended conjugation, an open-shell singlet biradical state could be more stable than the closed-shell state. We verified this hypothesis and elucidated the electronic state of *ZZ-ZZ*-**8**† using DFT calculations. Although a stable structure was observed for the closed-shell (CS) state, a solution could not be obtained for the open-shell (OS) singlet state using the broken-symmetry method, suggesting a significant contribution from the closed-shell configuration. Furthermore, SCF stability analysis was also performed using the geometry-optimized CS structure, and revealed that the obtained CS solution was stable. To quantitatively discuss this, the diradical character (y_0) was calculated based on the finite temperature DFT (FT-DFT),[41,42] yielding a value of 0.078, which was close to but not exactly zero. This finding indicated that the closed-shell contribution was predominant in *ZZ-ZZ*-**8**.

Therefore, we considered that the final cyclization reaction proceeds in the closed-shell state of *ZZ-ZZ*-**8**, via a 16π electrocyclic reaction. We then computationally evaluated the cyclization reaction at the ωB97X–D4[43,44]/def2-TZVP level (Figure 11). Transition state searches and activation energy estimation were conducted for *ZZ-ZZ*-**8**† considering only the CS state. Based on the NMR analysis of product **3** mentioned earlier and the Woodward–Hoffmann rule (16π electrocyclic reactions should proceed in a conrotatory manner), the configuration of **3** was considered to be *anti*. The ΔG value between the product (i.e., *anti*-**3**†) and the reactant (i.e., *ZZ-ZZ*-**8**†) were found to be

Table 1. Summary of the conformation analysis **8**† by the CENSO/CREST program.

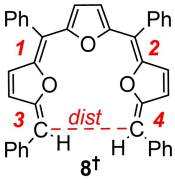

8†

Configurations *1,2,3,4*	No. of conformers[a]	Boltzmann weight[b] (%)	ΔG[c] (kcal/mol)	*dist*[c,d] (Å)
ZZZZ	13	91.6	0	3.707
ZZZE	17	1.2	2.13	3.193
ZZEE	45	0	4.68	3.134
EZZZ	12	6.6	0.57	6.150
EZZE	31	0.1	4.45	12.768
EZEZ	11	0.4	2.72	6.310
EZEE	142	0	7.05	6.558
EEZZ	10	0.1	3.45	10.014
EEZE	46	0	5.97	10.090
EEEE	75	0	9.07	10.145

[a] Obtained by default threshold settings. [b] All obtained conformers are considered. [c] For the most stable conformers. [d] Distance between the carbons involved in bond formation.

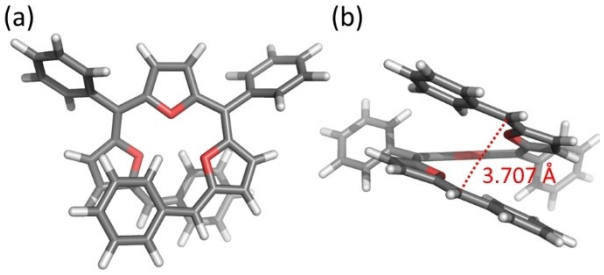

Figure 10. (a) Top, and (b) side views of most stable conformer of *ZZ-ZZ*-**8**†.

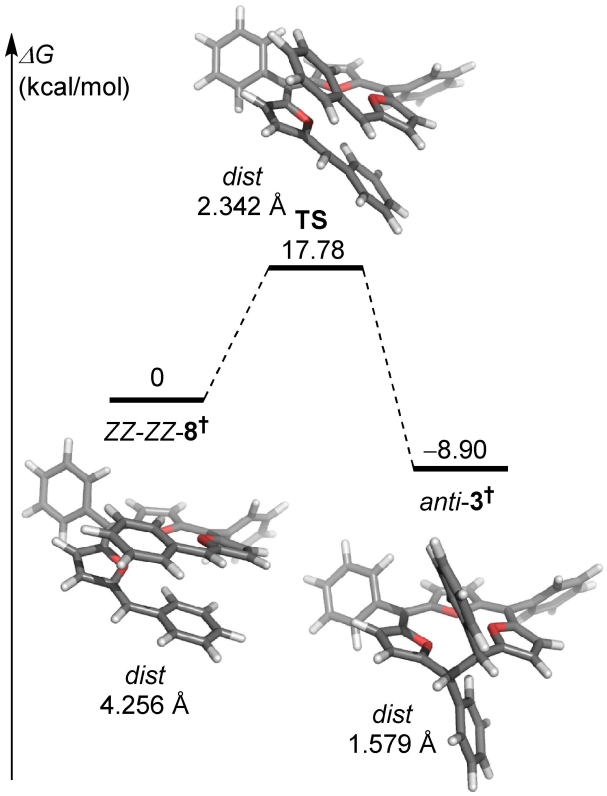

Figure 11. Potential energy surface of cyclization reaction of *ZZ-ZZ*-**8**† affording *anti*-**3**† computed at the ωB97X–D4/def2-TZVP level. Distance between the carbons involved in bond formation (*dist*) for each structure is also shown.

−8.90 kcal/mol, indicating that the reaction proceeded spontaneously. Only one transition state was observed in the cyclization reaction. The activation free energy $\Delta G^{\ddagger}$ was estimated to be 17.78 kcal/mol, suggesting that the cyclization reaction was feasible at room temperature.

The cyclization reaction to obtain **3** is suggested to proceed via a 16π electrocyclic reaction involving a linear-conjugated intermediate. Typically, electrocyclic reactions involve systems with fewer than 14π electrons.[45] To our knowledge, there have been only two examples of electrocyclization reactions involving more than 14π electron (16π[46] and 18π[47]). Very recently, 16π electrocyclic reaction mechanism was proposed through theoretical calculations[45] for one of the bacteriochlorin formation reaction.[46] Our findings expand the understanding of high-order electrocyclic reactions and open new possibilities for the design and synthesis of complex macrocyclic systems.

Conclusions

In conclusion, we have synthesized and characterized the first example of a stable trioxa[16]triphyrin(2.1.1) **1**, a 16π antiaromatic contracted porphyrinoid. X-ray crystallographic analysis of **1** revealed a nearly planar structure with a distinct bond-length alternation pattern. The antiaromaticity of **1** was confirmed through spectroscopic and computational studies.

Electrochemical investigations demonstrated reversible oxidation behavior and a small HOMO–LUMO gap of **1**, consistent with its antiaromatic nature. Remarkably, chemical oxidation of **1** afforded an aromatic 14π triphyrin(2.1.1) dication **7**$^{2+}$.

Quantum chemical calculations suggest that the key cyclization step from intermediate **4** to **3** proceeds via a 16π electrocyclic reaction involving a linear-conjugated intermediate **8**. This unique reaction expands the understanding of high-order pericyclic processes, which are rarely observed.

The synthesis and comprehensive characterization of trioxa[16]triphyrin(2.1.1) **1** represent a significant advancement in antiaromatic porphyrinoids. This study expands the scope of accessible antiaromatic-containing porphyrinoids and provides valuable insights into their structural, spectroscopic, and electrochemical properties. These findings underscore the potential of core modification strategies, such as heteroatom substitution, for the rational design of novel antiaromatic systems with tunable properties. The discovery of the rare 16π electrocyclic reaction also contributes to the understanding of high-order pericyclic processes and may inspire new synthetic strategies for complex macrocyclic compounds.

Supporting Information Summary

The authors have cited additional references within the Supporting Information (Ref. [48–57]). Deposition Number href="https://www.ccdc.cam.ac.uk/services/structures?id=doi:10.1002/chem.202403097">2336646 (for **1**) contains the supplementary crystallographic data for this paper. These data are provided free of charge by the joint Cambridge Crystallographic Data Centre and Fachinformationszentrum Karlsruhe href="http://www.ccdc.cam.ac.uk/structures">Access Structures service.

Acknowledgements

This work was supported by JSPS KAKENHI Grant Number JP19H02688, and Iketani Science and Technology Foundation (No. 0361035-A). We thank Dr. Yosuke Tani (Osaka University) and Prof. Dr. Takuji Ogawa (Osaka University) for helpful discussion. We are grateful to Prof. Rainer Herges (Christian-Albrechts-Universität, Kiel, Germany) for providing the AICD 3.0.4 program. The measurements were performed at the Analytical Instrument Facility, Graduate School of Science, Osaka University. The computation was performed using Research Center for Computational Science, Okazaki, Japan (Projects: 24-IMS-C238, 23-IMS-C224, 22-IMS-C217, and 21-IMS-C218).

Conflict of Interests

The authors declare no conflict of interest.

Data Availability Statement

The data that support the findings of this study are available in the supplementary material of this article.

Keywords: Antiaromaticity · Aromaticity · Triphyrin · Porphyrinoids · Electrocyclic reactions

[1] S. Hiroto, H. Shinokubo, in *Handbook of Porphyrin Science Volume 37: Synthesis and Reactivity of Exotic Porphyrinoids* (Eds: K. M. Kadish, K. M. Smith, R. Guilard), World Scientific Publishing, Singapore, Singapore **2016**, pp. 233–302.
[2] J. L. Sessler, D. Seidel, *Angew. Chem. Int. Ed.* **2003**, *42*, 5134–5175.
[3] S. Saito, A. Osuka, *Angew. Chem. Int. Ed.* **2011**, *50*, 4342–4373.
[4] A. Osuka, S. Saito, *Chem. Commun.* **2011**, *47*, 4330–4339.
[5] B. K. Reddy, A. Basavarajappa, M. D. Ambhore, V. G. Anand, *Chem. Rev.* **2017**, *117*, 3420–3443.
[6] P. Pushpanandan, M. Ravikanth, *Chem. Rec.* **2022**, *22*, e202200144.
[7] T. Ito, Y. Hayashi, S. Shimizu, J.-Y. Shin, N. Kobayashi, H. Shinokubo, *Angew. Chem. Int. Ed.* **2012**, *51*, 8542–8545.
[8] C. S. Wannere, D. Moran, N. L. Allinger, B. A. Hess Jr., L. J. Schaad, P. von R. Schleyer, *Org. Lett.* **2003**, *5*, 2983–2986.
[9] M. Jirásek, M. Rickhaus, L. Tejerina, H. L. Anderson, *J. Am. Chem. Soc.* **2021**, *143*, 2403–2412.
[10] S. Shimizu, *Chem. Rev.* **2017**, *117*, 2730–2784.
[11] G. Kaur, M. Ravikanth, in *Advances in Heterocyclic Chemistry* (Eds: E. F. V. Scriven, C. A. Ramsden), Elsevier, **2023**, pp. 171–231, Doi: 10.1016/bs.aihch.2022.11.003.
[12] Z.-L. Xue, Z. Shen, J. Mack, D. Kuzuhara, H. Yamada, T. Okujima, N. Ono, X.-Z. You, N. Kobayashi, *J. Am. Chem. Soc.* **2008**, *130*, 16478–16479.
[13] M. Pawlicki, K. Hurej, L. Szterenberg, L. Latos-Grażyński, *Angew. Chem. Int. Ed.* **2014**, *53*, 2992–2996.
[14] M. Pawlicki, M. Garbicz, L. Szterenberg, L. Latos-Grażyński, *Angew. Chem. Int. Ed.* **2015**, *54*, 1906–1909.
[15] K. Bartkowski, M. Dimitrova, P. J. Chmielewski, D. Sundholm, M. Pawlicki, *Chem. Eur. J.* **2019**, *25*, 15477–15482.
[16] K. Bartkowski, M. Pawlicki, *Angew. Chem. Int. Ed.* **2021**, *60*, 9063–9070.
[17] D. Kuzuhara, S. Kawatsu, W. Furukawa, H. Hayashi, N. Aratani, H. Yamada, *Eur. J. Org. Chem.* **2018**, 2122–2129.
[18] K. N. Panda, R. Sengupta, A. Kumar, M. Ravikanth, *J. Org. Chem.* **2021**, *86*, 3778–3784.
[19] T. Chatterjee, V. S. Shetti, R. Sharma, M. Ravikanth, *Chem. Rev.* **2017**, *117*, 3254–3328.
[20] X. Zhan, Y. Jin, D. Qi, T. Sun, J. Jiang, *Chem. Eur. J.* **2022**, *28*, e202201125.
[21] J. S. Reddy, V. G. Anand, *J. Am. Chem. Soc.* **2008**, *130*, 3718–3719.
[22] D. Kuzuhara, Y. Sakakibara, S. Mori, T. Okujima, H. Uno, H. Yamada, *Angew. Chem. Int. Ed.* **2013**, *52*, 3360–3363.
[23] K. N. Panda, K. G. Thorat, M. Ravikanth, *J. Org. Chem.* **2018**, *83*, 12945–12950.
[24] G. Kaur, M. Ravikanth, *Chem. Asian J.* **2022**, *17*, e202200531.
[25] D. Kuzuhara, H. Yamada, Z. Xue, T. Okujima, S. Mori, Z. Shen, H. Uno, *Chem. Commun.* **2011**, *47*, 722–724.
[26] K. Singh, T. S. Virk, J. Zhang, W. Xu, D. Zhu, *Chem. Commun.* **2012**, *48*, 121–123.
[27] W. Wang, B. Ji, Y. Zhang, *J. Phys. Chem. A* **2009**, *113*, 8132–8135.
[28] C. B. Aakeroy, D. L. Bryce, G. R. Desiraju, A. Frontera, A. C. Legon, F. Nicotra, K. Rissanen, S. Scheiner, G. Terraneo, P. Metrangolo, G. Resnati, *Pure Appl. Chem.* **2019**, *91*, 1889–1892.
[29] T. Fellowes, B. L. Harris, J. M. White, *Chem. Commun.* **2020**, *56*, 3313–3316.
[30] P. R. Varadwaj, *Molecules* **2019**, *24*, 3166.
[31] P. R. Varadwaj, A. Varadwaj, H. M. Marques, P. J. MacDougall, *Phys. Chem. Chem. Phys.* **2019**, *21*, 19969–19986.
[32] T. Fellowes, B. L. Harris, J. M. White, *Chem. Commun.* **2020**, *56*, 3313–3316.
[33] Q. Zhang, K. Luo, W. Zhou, A. Li, Q. He, *J. Am. Chem. Soc.* **2024**, *146*, 3635–3639.
[34] P. V. R. Schleyer, C. Maerker, A. Dransfeld, H. Jiao, N. J. R. van Eikema Hommes, *J. Am. Chem. Soc.* **1996**, *118*, 6317–6318.
[35] C. Corminboeuf, P. von R. Schleyer, R. Puchta, C. S. Wannere, Z. Chen, *Chem. Rev.* **2005**, *105*, 3842–3888.
[36] D. Geuenich, K. Hess, F. Köhler, R. Herges, *Chem. Rev.* **2005**, *105*, 3758–3772.
[37] T. Kawase, C. Wei, N. Ueno, M. Oda, *Chem. Lett.* **1994**, *23*, 1901–1904.
[38] S. Grimme, F. Bohle, A. Hansen, P. Pracht, S. Spicher, M. Stahn, *J. Phys. Chem. A* **2021**, *125*, 4039–4054.
[39] P. Pracht, F. Bohle, S. Grimme, *Phys. Chem. Chem. Phys.* **2020**, *22*, 7169–7192.
[40] P. Pracht, S. Grimme, C. Bannwarth, F. Bohle, S. Ehlert, G. Feldmann, J. Gorges, M. Müller, T. Neudecker, C. Plett, S. Spicher, P. Steinbach, P. A. Wesołowski, F. Zeller, *J. Chem. Phys.* **2024**, *160*, 114110.
[41] C. A. Bauer, A. Hansen, S. Grimme, *Chem. Eur. J.* **2017**, *23*, 6150–6164.
[42] Z. Chen, W. Li, M. A. Sabuj, Y. Li, W. Zhu, M. Zeng, C. S. Sarap, M. M. Huda, X. Qiao, X. Peng, D. Ma, Y. Ma, N. Rai, F. Huang, *Nat. Commun.* **2021**, *12*, 5889.
[43] J.-D. Chai, M. Head-Gordon, *Phys. Chem. Chem. Phys.* **2008**, *10*, 6615.
[44] E. Caldeweyher, S. Ehlert, A. Hansen, H. Neugebauer, S. Spicher, C. Bannwarth, S. Grimme, *J. Chem. Phys.* **2019**, *150*, 154122.
[45] A. de Cózar, A. Arrieta, I. Arrastia, F. P. Cossío, *ChemPlusChem* **2023**, *88*, e202300482.
[46] P. A. Jacobi, H. L. Brielmann, M. Chiu, I. Ghosh, S. I. Hauck, S. Lanz, S. Leung, Y. Li, H. Liu, F. Löwer, W. G. O'Neal, D. Pippin, E. Pollina, B. A. Pratt, F. Robert, W. P. Roberts, C. Tassa, H. Wang, *Heterocycles* **2010**, *82*, 1029.
[47] A. Beck, L. Knothe, D. Hunkler, H. Prinzbach, *Tetrahedron Lett.* **1982**, *23*, 2431–2434.
[48] G. M. Sheldrick, *Acta Crystallogr. Sect. A: Found. Adv.* **2015**, *71*, 3–8.
[49] G. M. Sheldrick, *Acta Crystallogr. A* **2007**, *64*, 112–122.
[50] G. M. Sheldrick, *Acta Crystallogr. B* **2015**, *71*, 3–8.
[51] M. J. Frisch, G. W. Trucks, H. B. Schlegel, G. E. Scuseria, M. A. Robb, J. R. Cheeseman, G. Scalmani, V. Barone, G. A. Petersson, H. Nakatsuji, X. Li, M. Caricato, A. V. Marenich, J. Bloino, B. G. Janesko, R. Gomperts, B. Mennucci, H. P. Hratchian, J. V. Ortiz, A. F. Izmaylov, J. L. Sonnenberg, D. Williams-Young, F. Ding, F. Lipparini, F. Egidi, J. Goings, B. Peng, A. Petrone, T. Henderson, D. Ranasinghe, V. G. Zakrzewski, J. Gao, N. Rega, G. Zheng, W. Liang, M. Hada, M. Ehara, K. Toyota, R. Fukuda, J. Hasegawa, M. Ishida, T. Nakajima, Y. Honda, O. Kitao, H. Nakai, T. Vreven, K. Throssell, J. A. Montgomery Jr., J. E. Peralta, F. Ogliaro, M. J. Bearpark, J. J. Heyd, E. N. Brothers, K. N. Kudin, V. N. Staroverov, T. A. Keith, R. Kobayashi, J. Normand, K. Raghavachari, A. P. Rendell, J. C. Burant, S. S. Iyengar, J. Tomasi, M. Cossi, J. M. Millam, M. Klene, C. Adamo, R. Cammi, J. W. Ochterski, R. L. Martin, K. Morokuma, O. Farkas, J. B. Foresman, D. J. Fox, Gaussian16, Revision C.01, Gaussian Inc., Wallingford, CT, **2016**.
[52] E. D. Glendening, J. K. Badenhoop, A. E. Reed, J. E. Carpenter, J. A. Bohmann, C. M. Morales, P. Karafiloglou, C. R. Landis, F. Weinhold, *NBO 7.0*, Theoretical Chemistry Institute, University of Wisconsin, Madison, WI **2018**.
[53] C. Bannwarth, E. Caldeweyher, S. Ehlert, A. Hansen, P. Pracht, J. Seibert, S. Spicher, S. Grimme, *Wiley Interdiscip. Rev. Comput. Mol. Sci.* **2021**, *11*, e1493.
[54] F. Neese, *Wiley Interdiscip. Rev. Comput. Mol. Sci.* **2022**, *12*, e1606.
[55] S. Grimme, A. Hansen, S. Ehlert, J.-M. Mewes, *J. Chem. Phys.* **2021**, *154*, 064103.
[56] F. Weigend, *Phys. Chem. Chem. Phys.* **2006**, *8*, 1057.
[57] F. Neese, F. Wennmohs, A. Hansen, U. Becker, *Chem. Phys.* **2009**, *356*, 98–109.

Manuscript received: August 17, 2024
Accepted manuscript online: September 5, 2024
Version of record online: October 29, 2024